

Self-Sensing Magnetic Bearings (Part II) – Effects of Saturation

Myounggyu D. Noh, Eric H. Maslen

Dept. of Mechanical, Aerospace, and Nuclear Engineering
Thornton Hall, University of Virginia
Charlottesville, VA 22903, USA
Tel: (804)-924-3292; FAX: (804)982-2246
e-mail: mn2n@virginia.edu, ehm7s@virginia.edu

Abstract

In our Part I paper, a nonlinear parameter estimation technique was presented by which the position of rotor supported by magnetic bearings can be deduced from the bearing current waveform. The estimator embedded an idealized model of the bearing inductance parameterized by the air gap. The performance of the estimator is limited by the quality of this embedded model. Magnetic saturation incurs a change of core reluctance which leads to an estimation error.

This paper investigates how saturation affects the performance of the position estimator based upon an idealized model. Identifying the effects of saturation is a prerequisite to exploring the possibility of using self-sensing magnetic bearings in high performance applications such as jet engines.

This work demonstrates that, in extreme cases, there is a sign reversal of the forward gain of the estimator due to saturation. A simple model of saturation is presented. This model enables one to qualitatively evaluate the effects of saturation on the performance of the estimator. A good agreement is observed between simulation and experiment.

The structure of a gap sensing estimator which accounts for this saturation effect is proposed and some stability issues which arise in its implementation are explored. This solution will require identification of the saturation nonlinearity in the actuator, but promises to recover the performance of previously reported estimators even in the face of fairly severe saturation.

1 Introduction

In the companion paper, a position estimator for magnetic bearing is developed using a nonlinear parameter estimation technique. The estimator embeds a linear simulation model of the inductance of the magnetic actuator. Consequently, the performance of the estimator depends fairly strongly on the quality of the model. When the actuator is operated at modest flux densities,

it is fairly easy to obtain a high quality simulation model because the air gap dominates the magnetic circuit reluctance. However, if the iron is saturated, the actual inductor differs from the simulation model significantly: the iron reluctance may exceed that of the gap. As a result, an estimator based on a linear (non-saturating) model will produce an incorrect estimate of the air gap if the iron begins to saturate.

This problem is fundamental to any self-sensing scheme: regardless of the actual implementation, they all fundamentally rely on the sensitivity of the coil electrical impedance to changes in the air gap. If the model for this sensitivity neglects the effect of saturation, then the estimate of the gap length extracted from the measured electrical impedance will be in error to an extent related to the degree of iron saturation. Thus, the problem needs to be addressed in order to realize self-sensing magnetic bearings in high performance applications such as aircraft jet engines.

When a switching amplifier is used to control the actuator, the amplitude of the switching “noise” is a direct measure of the electrical impedance of the actuator coil. If the amplitude is corrected for variations in amplifier duty cycle and power supply voltage (as discussed in Part I), the gain of the resulting signal to variations in air gap is a function of the air gap reluctance and the reluctance of the core material. At low flux levels, the core reluctance is independent of the rotor position and any reduction in air gap length produces an *increase* in coil electrical impedance. As the nominal coil current increases, however, a correlation appears between rotor movements and the core reluctance. If the rotor moves toward the stator, the reduction in the air gap produces an increase in flux density. Consequently, the core reluctance increases. This increase in core reluctance tends to offset the reduction in air gap reluctance which produces the measure of air gap. In the extreme, the sensitivity of core reluctance can actually exceed that of the air gap with the result that the overall electrical impedance actually *decreases* with decreasing air gap, producing a sign

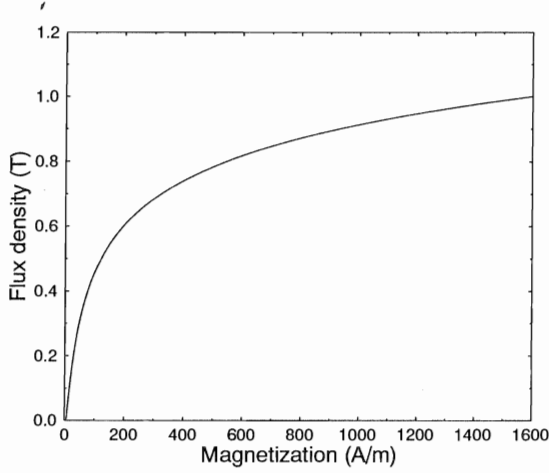


Figure 1: Saturation model

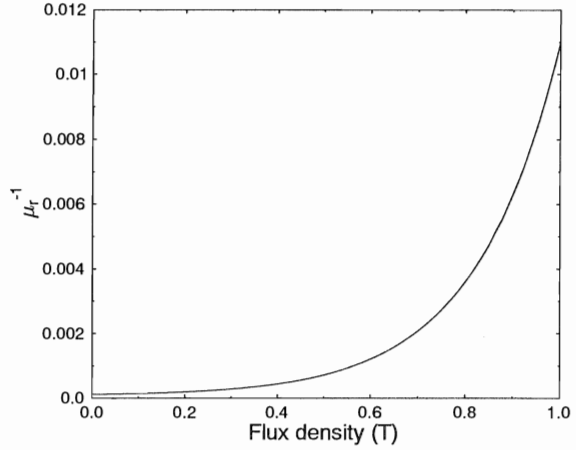


Figure 2: Inverse of relative permeability

reversal in sensitivity.

In order to explore this phenomenon and to develop a theoretical framework which can explain the experimental results, a simple model of saturation is presented. This model allows qualitative evaluation of the effects of saturation on the performance of the estimator. Numerical results are compared with the experimental data. Finally, suggestions are made to improve the estimator under saturation.

2 Saturation Model

To evaluate the effects of saturation, a proper saturation model is necessary. For this purpose, a number of nonlinear hysteresis models are available in the literature (notably by Jiles [1] or by Hodgdon [2]). In this work, however, a simple nonlinear saturation model is used. The model is described by

$$H = \frac{B}{\mu_o \mu_r^o} + \frac{\sigma}{\mu_o} \left(1 - \frac{1}{\mu_r^o} \right) \log \left[1 + \eta \cdot e^{(B-B_s)/\sigma} \right] \quad (1)$$

where μ_r^o is the nominal relative permeability of the core iron. In (1), η and σ are the parameters of the model, which can be readily obtained from experimental data. The core reluctance is directly proportional to the inverse of relative permeability, μ_r^{-1} . By differentiating (1) with respect to B ,

$$\mu_r^{-1} = \frac{1}{\mu_r^o} + \left(1 - \frac{1}{\mu_r^o} \right) \frac{\eta \cdot e^{(B-B_s)/\sigma}}{1 + \eta \cdot e^{(B-B_s)/\sigma}} \quad (2)$$

Figure 1 shows a $B-H$ curve produced by this model. As illustrated in Figure 2, μ_r^{-1} increases rapidly at high flux density.

3 Saturation Effect

For the sake of simplicity, a horseshoe electro-magnet illustrated in Figure 3 is examined to show the effects of

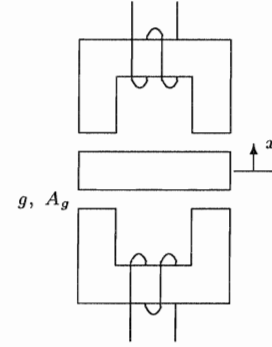


Figure 3: A horseshoe electro-magnet

magnetic saturation on the performance of self-sensing. The analysis presented hereafter can easily be extended for general n -pole magnetic bearings.

It is shown in Part I that the amplitude of the demodulated switching waveform of the bottom coil is a function of the air gap reluctance and the core reluctance:

$$u = \kappa(r_g + r_c) \quad (3)$$

where

$$r_g = \frac{2(g+x)}{\mu_o A_g}, \quad r_c = \frac{l_c}{\mu_o \mu_r A_g} \quad (4)$$

At low flux levels, the core reluctance, r_c , is negligible compared to r_g , as the relative permeability of the core material is large (usually 1000 ~ 5000). Therefore, the output u can be assumed linear in the displacement x . In other words, the sensitivity of u with respect to x ,

$$S_x^u \doteq \frac{\partial u}{\partial x} = \frac{2\kappa}{\mu_o A_g} \quad (5)$$

is essentially constant. When the core iron becomes magnetically saturated, this assumption is no longer valid.

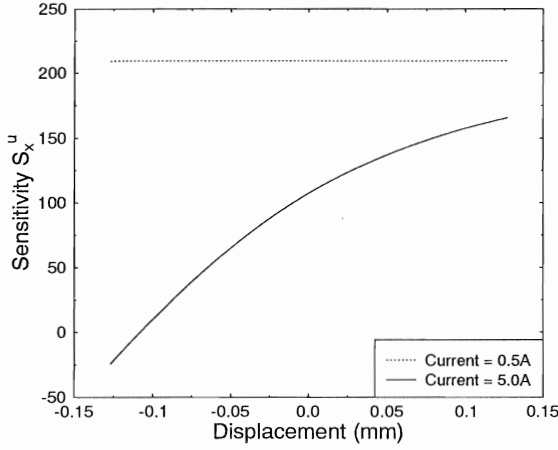


Figure 4: Variations of sensitivity with respect to gap displacement

The core reluctance is, in fact, a function of the air gap. This functional relationship becomes increasingly noticeable at high flux levels.

Using the chain rule, the sensitivity of core reluctance with respect to x can be written as

$$\frac{\partial r_c}{\partial x} = \frac{\partial r_c}{\partial H_c} \frac{\partial H_c}{\partial x} \quad (6)$$

where H_c is the magnetization (or field intensity) applied to the core iron. Assuming that the coil current is constant, the second term in (6) on the right hand side can be obtained by differentiating Ampère's loop law with respect to x :

$$\frac{\partial H_c}{\partial x} = -\frac{B}{\mu_o(2\mu_r g + l_c)} \quad (7)$$

where μ_r is the differential permeability and is defined as

$$\mu_r = \frac{1}{\mu_o} \frac{\partial B}{\partial H_c} \quad (8)$$

The sensitivity S_x^u is then

$$S_x^u = \frac{\kappa}{\mu_o A_g} \left[2 + \frac{(\partial^2 B / \partial H_c^2) l_c}{\mu_o^2 \mu_r^2} \cdot \frac{B}{2\mu_r g + l_c} \right] \quad (9)$$

From (9), it is clear that S_x^u is a nonlinear function of x . Assuming a constant nominal current in the coil (switching about a fixed point), it is possible to see how the sensitivity changes using the saturation model given in the previous section. Figure 4 illustrates the variations of the sensitivity at two different current levels. In this plot, a negative displacement corresponds to a reduction in the air gap length, with the gap going to zero at about -0.3 mm. As expected, the sensitivity at low current level (thus low flux level) remains constant, whereas it decreases rapidly at small air gaps if the current is high.

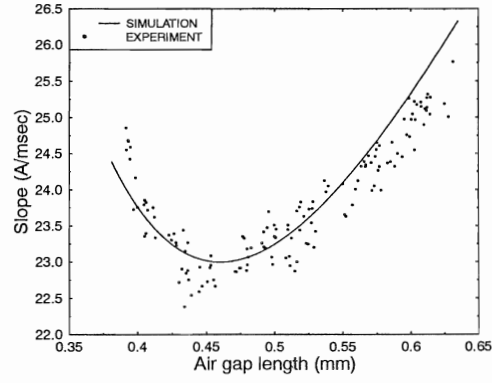


Figure 5: Experimentally measured current rate

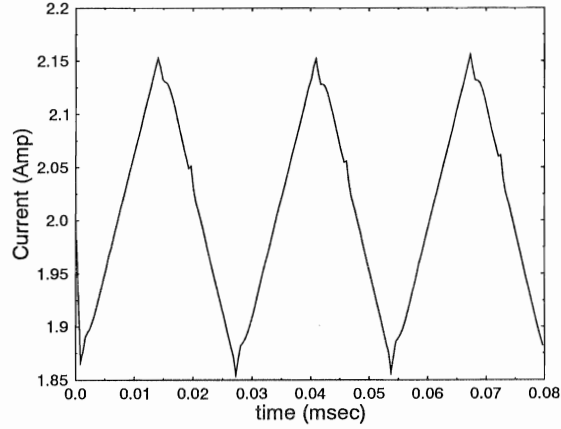


Figure 6: A typical current switching waveform

Indeed, at a current of five amps and displacements in excess of 0.12 mm, the sensitivity reverses sign.

The sensitivity change due to saturation is also verified by experiments. In Figure 5, experimentally measured current rates (di/dt) show good agreements with the simulation results. To generate this data, the journal of the experimental apparatus described in Part I was clamped at a range of positions (as reflected in the abscissa of Figure 5) and the switching current waveform was acquired using a high speed digital storage oscilloscope. Figure 6 illustrates a typical waveform. The slope of the rising portion of the waveform was measured and averaged over ten cycles to produce the data shown in Figure 5.

4 Revised Estimator

To achieve self-sensing in high-performance applications, the problem due to saturation needs to be resolved. A simple palliative is to use a pair of self-sensing circuits on opposing sides of the shaft. Assuming that only

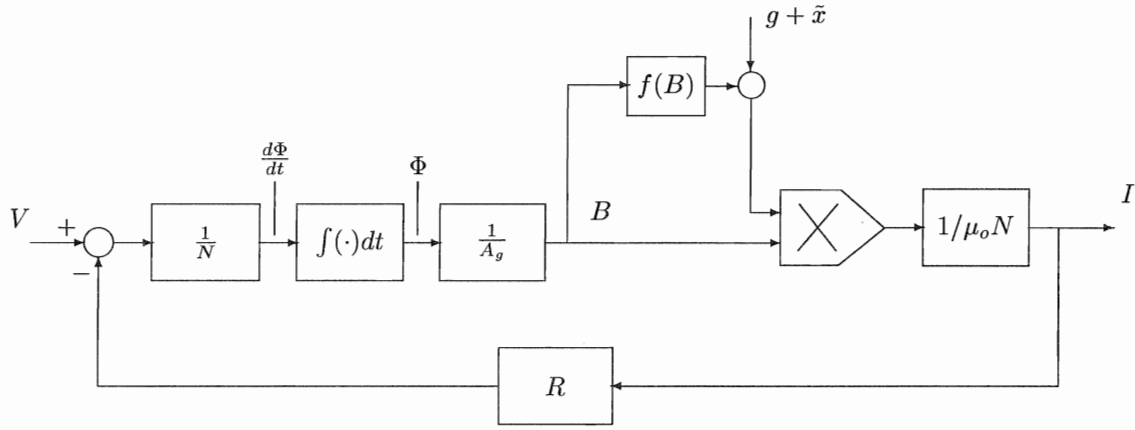


Figure 7: A revised inductor model

one side of the magnetic circuit is saturated at a given instant, then only one of the two sensors suffers significantly from saturation effects at a given instant. Examination of the currents in the two opposed coil sets makes it quite simple to *select* the appropriate sensor and always extract the shaft position from the unsaturated side.

The primary problem with this selection approach is that the transition from sensing with one side to sensing with the other is awkward and may be expected to lead to sensitive calibration and offset requirements in order to avoid signal discontinuity at the cross-over point. Further, if *both* sides of the circuit simultaneously exhibit some degree of saturation, then neither side will produce an accurate measure of the air gap. A better solution relies on a true differential sensing scheme coupled with including a saturation model into the embedded inductor simulation.

Faraday's law states that

$$V - IR = NA_g \frac{dB}{dt} \quad (10)$$

Furthermore, by Ampère's loop law,

$$I = \frac{1}{\mu_o N} \left(2g + \frac{l_c}{\mu_r} \right) B \quad (11)$$

The relative permeability (at a given frequency) depends only upon B .

$$\frac{l_c}{\mu_r} = f(B) \quad (12)$$

Thus, a new simulation model including saturation can be built as shown in Figure 7. Note that this model includes the back-emf term (i.e. velocity effects) which was neglected in the linear simulation model presented in Part I.

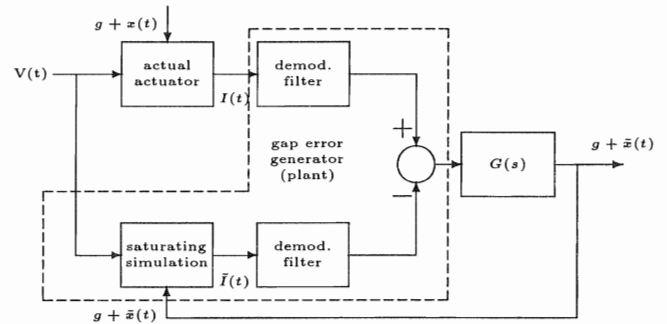


Figure 8: Possible estimator structure with saturating simulation

5 Estimator Loop with Saturation Model

Assuming that the saturation effects can be properly simulated by the nonlinear function $f(B)$, the model presented in Figure 7 should reproduce the measured switching current waveform when the correct journal position is impressed as \tilde{x} even when the displacements and average currents are quite high, implying magnetic saturation. Given this, it is tempting to simply embed this nonlinear simulation model into the parameter (\tilde{x}) servo loop described in Part I and thereby realize a self-sensing discriminator which works even when the actuator iron is saturated.

Representing the simulation block by the three port element depicted in Figure 8, the output would be demodulated using the forward path filter described in Part I: a high pass element followed by a rectifier followed by a low pass element to yield a low frequency signal closely related to the air gap length (but modulated by the amplifier duty cycle and power supply voltage). The measured current waveform from the actuator passes through the same demodulation filter and the error between the

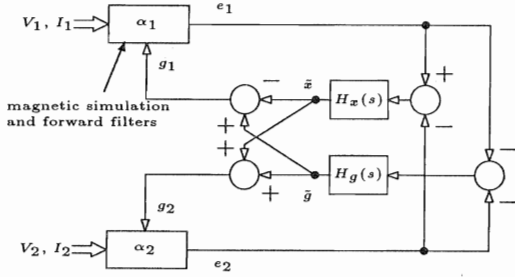


Figure 9: Differential estimator structure

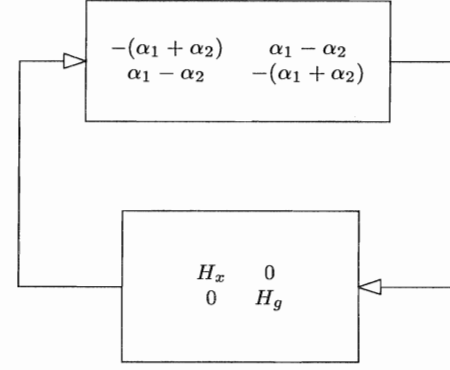


Figure 10: Stability model for the differential estimator

two resulting signals is used to update the estimate of the rotor position (total air gap, $g + \hat{x}$).

Assuming that the duty cycle and amplitude of $V(t)$ are constant, the effective low frequency gain (ratio of filter output to gap estimate) of the simulation and demodulation filter is described by Figure 4. Denoting this gain as α , stability of the estimator is ensured as long as the characteristic function $1 + \alpha G(s)$ has its roots in the left half of the complex plane. The problem is that, if $G(s)$ is designed for stability at nominal values of α (the dotted line in Figure 4) then the loop will not be stable for the negative values of α which arise when the iron is saturated.

6 Differential Estimator

An appealing solution to this problem is provided by developing a differential sensor scheme as depicted in Figure 9. This differential scheme estimates both the journal position, x , and the nominal radial air gap, g . The latter is assumed to vary slowly with time due to centripetal stress and/or thermal deformation. The three port elements labeled *magnetic simulation and forward filters* are an encapsulation of the block surrounded by the dashed line in Figure 8. As indicated, it is assumed that the error signal e_1 is generated by one of a pair of opposed magnetic circuits while the error signal e_2 is generated by the other (see Figure 3). With this assumption, it is reasonable to assume that only one of the structures is saturated at any given time and that the other is operating near to the nominal properties.

Stability of this system is ensured if the eigenvalues of the block system illustrated in Figure 10 are in the left half plane. With the assumption that only one circuit is saturated at any given time, we can assume that one filter gain is at the nominal value, α_0 (again, the dotted line in Figure 4), while the other gain is diminished by an amount δ :

$$\alpha_1 = \alpha_0, \quad \alpha_2 = \alpha_0 - \delta \quad : \quad 0 < \delta < 1.1\alpha_0$$

or

$$\alpha_1 = \alpha_0 - \delta, \quad \alpha_2 = \alpha_0 \quad : \quad 0 < \delta < 1.1\alpha_0$$

where the factor of 1.1 is estimated from Figure 4. Stability for one case implies stability for the other, so we

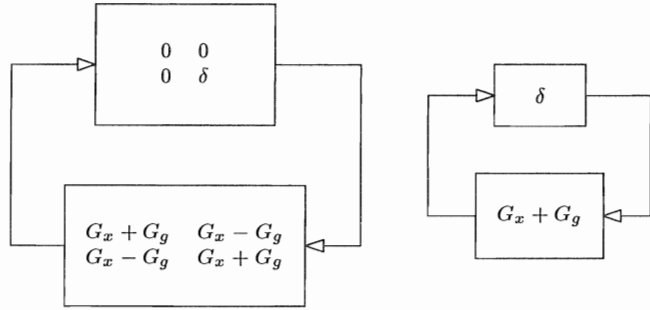


Figure 11: Differential estimator stability model with uncertainty isolated

focus on the first case in the sequel.

The block diagram shown in Figure 10 can be manipulated into the much simpler form shown on the left side of Figure 11 where the nominal feedback loops have been subsumed into the closed loop transfer functions G_x and G_g and the saturation uncertainty δ has been conveniently isolated:

$$G_x = \frac{H_x}{1 + 2\alpha_0 H_x}, \quad G_g = \frac{H_g}{1 + 2\alpha_0 H_g}$$

Noting that G_x and G_g are assumed stable (the nominal estimator is stable) and that

$$\begin{bmatrix} 0 & 0 \\ 0 & \delta \end{bmatrix} = \begin{bmatrix} 0 \\ 1 \end{bmatrix} \delta \begin{bmatrix} 0 & 1 \end{bmatrix}$$

the stability analysis need only be carried out for the simple problem indicated on the right side of Figure 11. Thus, the stability question can be bounded using the small gain theorem [3]: the estimator is stable as long as

$$|\delta(G_x + G_g)|_{j\omega} < 1 \quad \forall \omega \in \mathbb{R}$$

The triangle inequality provides

$$|\delta(G_x + G_g)|_{j\omega} < |\delta G_x|_{j\omega} + |\delta G_g|_{j\omega}$$

Assuming that G_x has a damping ratio of at least 0.707,

$$|\delta G_x| < 0.55$$

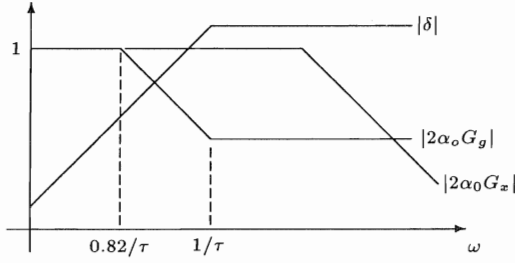


Figure 12: Magnitude bounds of $2\alpha_0 G_x(j\omega)$, $2\alpha_0 G_g(j\omega)$, and $\delta(j\omega)$.

Thus, stability is ensured if

$$|\delta G_g| < 0.45$$

The gains of $2\alpha_0 H_x$ and $2\alpha_0 H_g$ will be much greater than 1.0 from DC out to the estimator bandwidth for the shaft position and the nominal gap, respectively. This means that, at DC,

$$|G_g|_{\omega=0} \approx \frac{1}{2\alpha}$$

Therefore, it is not possible to satisfy the small gain theorem if δ can be as large as $0.9\alpha_0$ at DC. That is, the estimator will begin to diverge from an accurate estimate either of x or of g_0 if saturation persists beyond some acceptable time scale.

Assuming that there is a reasonable estimate of the greatest likely duration of saturation, this stability problem can be avoided simply by making the dominant time constant of the gap estimate, G_g , be greater than this expected saturation dwell. That is, assume that δ is bounded by

$$|\delta| < \left| \frac{1.1\alpha_0 s}{s + 1/\tau} \right|$$

then the estimator will be stable as long as

$$|G_g| < \left| \frac{0.45 s + 1/\tau}{1.1 \alpha_0 s} \right|$$

where s is the Laplace variable. Since it is already established that good convergence at DC dictates a DC gain of $1/2\alpha_0$, we revise to the more conservative bound

$$|G_g| < \left| \frac{0.45}{1.1} \frac{s + 1/\tau}{\alpha_0(s + 0.82/\tau)} \right| \quad (13)$$

Figure 12 illustrates the bounds of $|2\alpha_0 G_g(j\omega)|$, $|2\alpha_0 G_x(j\omega)|$, and $|\delta(j\omega)|$.

7 Discussion

The reason that the estimate of the nominal gap must be severely bandwidth-limited in order to maintain stability in the face of magnetic saturation is that the mag-

netic circuit (sensor) on one side of the system may produce little or no usable information in extreme saturation. Thus, only one piece of information can be extracted from the pair: either nominal gap or shaft position. Under the assumption that saturation is a momentary phenomenon, this loss of information is intermittent. Thus, it is always possible to obtain a good estimate of the shaft position, x , but caution must be exercised in estimating the nominal gap, g . This caution is acceptable because it is assumed that the mechanisms leading to variation in nominal gap function vary slowly relative to those which lead to variation in shaft position.

It is important to note that the reduction in stability margin which necessarily accompanies saturation does not imply a loss of estimation accuracy. As long as the saturation model embedded by $f(B)$ is accurate, the estimates of both x and g should be precise, subject to the bandwidth limitations of G_x and G_g .

8 Conclusion

In this work, the effects of saturation on self-sensing has been investigated. It has shown that the sensitivity of the estimator changes due to saturation, resulting in incorrect estimation. If a bearing is generating a large force with small air gap, the sensitivity may undergo a sign reversal which causes the estimator to be unstable. In this work, we also proposed a differential estimator that includes a saturation model. This estimator simultaneously estimates the displacement and the gap. We explored the stability of the proposed estimator using the small gain theorem and demonstrated that wide-band estimation of journal motion requires gap estimator to be bandwidth-limited in order to be stable. The proposed estimator requires further investigation through simulation and experiments.

References

- [1] D. C. Jiles and D. L. Atherton, "Theory of ferromagnetic hysteresis," *Journal of Magnetism and Magnetic Materials*, vol. 61, pp. 48–60, 1986.
- [2] M. L. Hodgdon, "Applications of a theory of ferromagnetic hysteresis," *IEEE Transactions on Magnetics*, vol. 24, pp. 218–221, January 1988.
- [3] H. K. Khalil, *Nonlinear Systems*. Macmillan Publishing Company, 1992.